

Mapping of the extinction in Giant Molecular Clouds using optical star counts

L. Cambr esy

Observatoire de Paris, D epartement de Recherche Spatiale, F-92195 Meudon Cedex, France

Abstract. This paper presents large scale extinction maps of most nearby Giant Molecular Clouds of the Galaxy (Lupus, ρ Ophiuchus, Scorpius, Coalsack, Taurus, Chamaeleon, Musca, Corona Australis, Serpens, IC 5146, Vela, Orion, Monoceros R1 and R2, Rosette, Carina) derived from a star count method using an adaptive grid and a wavelet decomposition applied to the optical data provided by the USNO-Precision Measuring Machine. The distribution of the extinction in the clouds leads to estimate their total individual masses M and their maximum of extinction. I show that the relation between the mass contained within an iso-extinction contour and the extinction is similar from cloud to cloud and allows the extrapolation of the maximum of extinction in the range 5.7 to 25.5 magnitudes. I found that about half of the mass is contained in regions where the visual extinction is smaller than 1 magnitude. The star count method used on large scale (~ 250 square degrees) is a powerful and relatively straightforward method to estimate the mass of molecular complexes. A systematic study of the all sky would lead to discover new clouds as I did in the Lupus complex for which I found a sixth cloud of about $10^4 M_{\odot}$.

Key words: ISM : clouds – ISM : dust, extinction – ISM : structure

1. Introduction

Various methods have been recently developed to estimate the mass of matter contained in giant molecular clouds (GMC) using millimetric and far infrared observations (Boulanger et al. 1998; Mizuno et al. 1998). Nevertheless, the mapping of the optical/near-infrared extinction, based on star counts still remain the most straightforward way to estimate the mass in form of dust grains. These maps can be usefully compared to longer wavelength emission maps in order to derive the essential physical parameters of the interstellar medium such as the gas to dust mass ratio, the clumpiness of the medium or the optical

and morphological properties of the dust grains. The star count method was first proposed by Wolf (1923) and has been applied to Schmidt plates during several decades. It consists to count the number of stars by interval of magnitudes (i.e. between $m - 1/2$ and $m + 1/2$) in each cell of a regular rectangular grid in an obscured area and to compare the result with the counts obtained in a supposedly unextinguished region. In order to improve the spatial resolution, Bok (1956) proposed to make count up to the completeness limiting magnitude ($m \leq m_{lim}$). Since the number of stars counted is much larger when compared to counts performed in an interval of 1 magnitude, the step of the grid can be reduced. Quite recently extinction maps of several southern clouds have been drawn by Gregorio Hetem et al. (1988) using this second method. Even more recently, Andreazza and Vilas-Boas (1996) obtained extinction map of the Corona Australis and Lupus clouds. Counts were done *visually* using a $\times 30$ magnification microscope. With the digitised Schmidt plates the star counts method can be worked out much more easily across much larger fields. The star count methods have also tremendously evolved thanks to the processing of digital data with high capacity computers. Cambr esy et al. (1997), for instance, have developed a counting method, for the DENIS data in the Chamaeleon I cloud, that takes advantage of this new environment. The aim of this paper is to apply this method to the optical plates digitised with the USNO-PMM in a sample of Giant Molecular Clouds to derive their extinction map (Vela, Fig. 1; Carina, Fig. 2; Musca, Fig. 3; Coalsack, Fig. 4; Chamaeleon, Fig. 5; Corona Australis, Fig. 6; IC 5146, Fig. 7; Lupus, Fig. 8; ρ Ophiuchus, Fig. 9; Orion, Fig. 11; Taurus, Fig. 12; Serpens, Fig. 13). The method is shortly described in Sect. 2. In Sect. 3, deduced parameters from the extinction map are presented and Sect. 4 deals with individual clouds.

2. Star counts

2.1. Method

The star counts method is based on the comparison of local stellar densities. A drawback of the classical method is that it requests a grid step. If the step is too small, this

may lead to empty cells in highly extinguished regions, and if it is too large, it results in a low spatial resolution. My new approach consists in fixing the number of counted stars per cell rather than the step of the grid. Since uncertainties in star counts follow a poissonian distribution, they are independent of the local extinction with an adaptive grid where the number of stars in each cell remains constant. Practically, I used a fixed number of 20 stars per cell and a filtering method involving a wavelet decomposition that filters the noise. This method has been described in more details by Cambr sy (1998).

Fig. 1. Extinction map of Vela from B counts (J2000 coordinates)

Fig. 2. Extinction map of Carina from R counts (J2000 coordinates)

Fig. 3. Extinction map of Musca from R counts (J2000 coordinates)

I have applied the method to 24 GMCs. Counts and filtering are fully automatic. Because of the wide field (~ 250 square degrees for Orion), the counts must be corrected for the variation of the background stellar density with galactic latitude. Extinction and stellar density are related by:

$$A_\lambda = \frac{1}{a} \log \left(\frac{D_{ref}(b)}{D} \right) \quad (1)$$

where A_λ is the extinction at the wavelength λ , D is the background stellar density, D_{ref} the density in the reference field (depending on the galactic latitude b), and a is defined by :

$$a = \frac{\log(D_{ref}) - cst.}{m_\lambda} \quad (2)$$

where m_λ is the magnitude at the wavelength λ .

Assuming an exponential law for the stellar density, $D_{ref}(b) = D_0 e^{-\alpha|b|}$, a linear correction with the galactic latitude b must be applied to the extinction value given by Eq. (1). The correction consists, therefore, in subtracting $\log[D_{ref}(b)] = \log(D_0) - \alpha|b| \log(e)$ to the extinction value $A_\lambda(b)$. This operation corrects the slope of $A_\lambda(b)$ which becomes close to zero, and set the zero point of extinction. All maps are converted into visual magnitudes assuming an extinction law of Cardelli et al. (1989) for which $\frac{A_B}{A_V} = 1.337$ and $\frac{A_R}{A_V} = 0.751$.

Here, the USNO-PMM catalogue (Monet 1996) is used to derive the extinction map. It results from the digitisation of POSS (down to -35° in declination) and ESO

plates ($\delta \leq -35^\circ$) in blue and red. Internal photometry estimators are believed to be accurate to about 0.15 magnitude but systematic errors can reach 0.25 magnitude in the North and 0.5 magnitude in the South. Astrometric error is typically of the order of 0.25 arcsecond. This accuracy is an important parameter in order to count only once those stars which are detected twice because they are located in the overlap of two adjacent plates.

All the extinction maps presented here have been drawn in greyscale with iso-extinction contours overlaid. On the right side of each map, a scale indicates the correspondence between colours and visual extinction, and the value of the contours. Stars brighter than the 4th visual magnitude (Hoffleit and Jaschek 1991) are marked with a filled circle.

2.2. Artifacts

Bright stars can produce *artifacts* in the extinction maps. A very bright star, actually, produces a large disc on the plates that prevents the detection of the fainter star (for example, α Crux in the Coalsack or *Antares* in ρ Ophiuchus, in Fig. 4 and 9, respectively). The magnitude of *Antares* is $m_V = 0.96$, and it shows up in the extinction map as a disc of 35' diameter which mimics an extinction of 8 magnitudes. Moreover *Antares* is accompanied of reflection nebulae that prevent source extraction. In Fig. 11 the well known Orion constellation is drawn over the map and the brighter stars appear. ϵ Ori (*Alnilam*) the central star of the constellation, free of any reflection nebula, is represented by a disc of $\sim 14'$ for a magnitude of $m_V = 1.7$. Fortunately, these artifacts can be easily identified when the bright star is isolated. When stars are in the line of sight of the obscured area, the circularity of a small extinguished zone is just an indication, but the only straightforward way to rule out a doubt is to make a direct visual inspection of the Schmidt plate.

Reflection nebulae are a more difficult problem to identified since they are not always circular. Each time it was possible, I chose the R plate because the reflection is much lower in R than in B . B plates were preferred when R plates showed obvious important defaults (e.g. edge of the plate).

2.3. Uncertainties

Extinction estimations suffer from intrinsic and systematic errors. Intrinsic uncertainties result essentially from the star counts itself. The obtained distribution follows a Poisson law for which the parameter is precisely the number of stars counted in each cell, i.e. 20. Equation (1) shows that two multiplicative factors, depending on which colour the star counts is done, are needed to convert the stellar density into visual extinction. These factors are a (the slope of the luminosity function (2)), and the conversion factor A_λ/A_V . For B and R band, the derived extinc-

Fig. 4. Extinction map of Coalsack from R counts (J2000 coordinates)**Fig. 5.** Extinction map of the Chamaeleon complex from B counts (J2000 coordinates)**Fig. 6.** Extinction map of Corona Australis from B counts (J2000 coordinates)

tion accuracies are $^{+0.29}_{-0.23}$ magnitudes and $^{+0.5}_{-0.4}$ magnitudes, respectively.

Also, for highly obscured region, densities are estimated from counts on large surfaces, typically larger than $\sim 10'$. It is obvious that, in this case, the true peak of extinction is underestimated since we have only an average value. The resulting effect on the extinction map is similar to the *saturation* produced by bright stars on Schmidt plates. This effect cannot be easily estimated and is highly dependant on the cloud (about ~ 80 magnitudes in ρ Ophiuchus, see Sect. 3.2).

Moreover, systematic errors due to the determination of the zero point of extinction are also present. Extinction mappings use larger areas than the cloud itself in order to estimate correctly the zero point. This systematic uncertainty can be neglected in most cases.

3. The extinction maps and the derived parameters

3.1. Fractal distribution of matter in molecular clouds

Fractals in molecular clouds characterize a geometrical property which is the dilatation invariance (i.e. self-similar fractals) of their structure. A fractal dimension in cloud has been first found in Earth's atmospheric clouds by comparing the perimeter of a cloud with the area of rain. Then, using *Viking* images, a fractal structure for Martian clouds has also been found. Bazell and D sert (1988) obtained similar results for the interstellar cirrus discovered by IRAS. Hetem and L pine (1993) used this geometrical approach to generate clouds with some statistical properties observed in real clouds. They showed that classical models of spherical clouds can be improved by a fractal modelisation which depends only on one or two free parameters. The mass spectrum of interstellar clouds can also be understood assuming a fractal structure (Elmegreen and Falgarone 1996). Larson (1995) went further, showing that the Taurus cloud also presents a fractal structure in the distribution of its young stellar objects.

Blitz and Williams (1997) claim, however, that clouds are no longer fractal since they found a characteristic size scale in the Taurus cloud. They showed that the Taurus cloud is not fractal for a size scale of 0.25-0.5 pc which may correspond to a transition from a turbulent outer envelope to an inner coherent core. This is not inconsistent with a fractal representation of the cloud for size scales greater

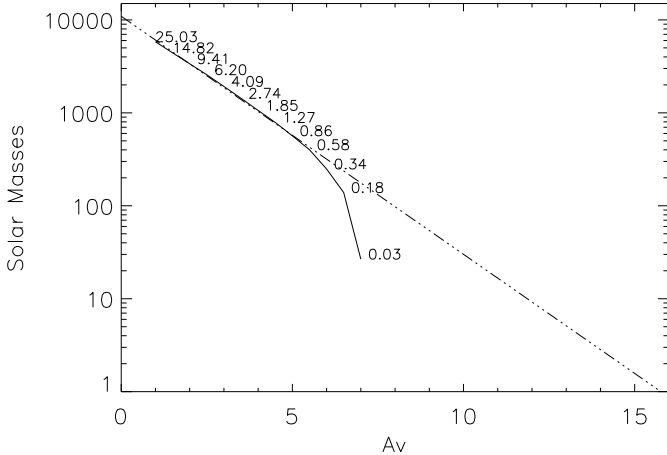
Table 1. Cloud properties. Distances are taken from literature, masses (expressed in solar masses) are defined by the regression line $\log M(A_V) = \log(M_{Tot}) + a \times A_V$, the maxima of extinction, A_V^m , is measured from star counts, and A_V^e , is extrapolated from the previous equation assuming a fractal structure and the last column is the value of the slope a

Cloud Name	d (pc)	A_V^m	A_V^e	M_{Tot}	Slope
Lupus I	100 ⁽¹⁾	5.3	7.1	10 ⁴	-0.56
Lupus II	100 ⁽¹⁾	3.8	5.7	80	-0.33
Lupus III	100 ⁽¹⁾	4.9	7.6	1150	-0.40
Lupus IV	100 ⁽¹⁾	5.3	7.0	630	-0.40
Lupus V	100 ⁽¹⁾	5.2	10.6	2500	-0.32
Lupus VI	100	4.8	7.0	10 ⁴	-0.57
ρ Ophiuchus	120 ⁽¹⁾	9.4	25.5	6600	-0.15
Scorpius	120	6.4	7.0	6000	-0.54
Taurus	140 ⁽²⁾	7.5	15.7	1.1 10 ⁴	-0.26
Coalsack	150 ⁽¹⁾⁽³⁾	6.6	6.3	1.4 10 ⁴	-0.63
Musca	150 ⁽¹⁾	5.7	10.1	550	-0.27
Chamaeleon III	150 ⁽⁴⁾	3.7	7.8	1300	-0.40
Chamaeleon I	160 ⁽⁴⁾	5.2	12.9	1800	-0.25
Corona-Australis	170 ⁽¹⁾	5.4	10.7	1600	-0.30
Chamaeleon II	178 ⁽⁴⁾	4.9	12.3	800	-0.22
Serpens	259 ⁽⁵⁾	10.1	???	???	???
IC 5146	400 ⁽⁶⁾	6.5	11.9	2900	-0.29
Vela	500 ⁽⁷⁾	4.0	???	???	???
Orion	500 ⁽⁸⁾	7.5	20.3	3 10 ⁵	-0.27
Crossbones	830 ⁽⁸⁾	4.4	10.4	7.3 10 ⁴	-0.47
Monoceros R2	830 ⁽⁸⁾	4.1	10.5	1.2 10 ⁵	-0.48
Monoceros R1	1600 ⁽⁹⁾	5.4	20.8	2.7 10 ⁵	-0.26
Rosette	1600 ⁽⁹⁾	8.4	20.4	5 10 ⁵	-0.28
Carina	2500 ⁽¹⁰⁾	8.3	82?	5.5 10 ⁵ ?	-0.07?

(1) : Knude and Hog (1998), (2) : Kenyon et al. (1994), (3) : Franco (1995), (4) : Whittet et al. (1997), (5) : Straizys et al. (1996), (6) : Lada et al. (1994), (7) : Duncan et al. (1996), (8) : Maddalena et al. (1986), (9) : Turner (1976), (10) : Feinstein (1995)

than 0.5 pc. Fractal in physics are defined over a number of decades and have *always* a lower limit.

Fractal structures in clouds can be characterized by a linear relation between the radius of a circle and the mass that it encompasses in a log-log diagram. Several definitions of fractal exist, and this definition can be written $M \propto L^D$, where L is the radius of the circle and D the fractal dimension of the cloud. The mass measured is, in

Fig. 7. Extinction map of IC5146 from R counts (J2000 coordinates)**Fig. 8.** Extinction map of the Lupus complex from B counts (J2000 coordinates)**Fig. 9.** Extinction map of ρ Ophiuchus and Scorpius clouds from R counts (J2000 coordinates)**Fig. 10.** Mass contained inside the iso-extinction contours versus the extinction (solid line), and regression line for the linear part. Annotations indicate the area in square degrees contained by the iso-extinction contours A_V .

fact, contained in a cylinder of base radius L and of undefined height H (because the cloud depth is not constant over the surface of the base of the cylinder). In our case, we are interested in the relation between the mass and the extinction. Since the extinction is related to the size H , which represents the depth of the cloud as defined above, we seek for a relation between mass and A_V (or H), L being now undefined. The logarithm of the mass is found to vary linearly with the extinction over a range of extinction magnitudes (Fig. 10). We have:

$$\log M = \log M_{Tot} + slope \times A_V \quad (3)$$

This result is compatible with a fractal structure of the cloud if $A_V \propto \log H$, i.e. if the density of matter follows a power law, which is, precisely, what is used in modelling interstellar clouds (Bernard et al. 1993).

3.2. Maximum of extinction

Fig. 10 shows the relation between iso-extinction contours and the logarithm of the mass contained inside these contours for the Taurus cloud (see extinction map in Fig. 12). The relation is linear for $A_V \lesssim 5.5$. For higher extinction, mass is deficient because the star count leads to underestimating the extinction. Indeed, for highly extinguished regions, the low number density of stars requires a larger area to pick up enough stars and estimate the extinction. The result is therefore an average value over a large area

in which the extinction is, in fact, greater. In the Taurus cloud, I found that this turn off occurs for a size of ~ 1.7 pc. According to Blitz and Williams (1997) a turn off toward higher masses should appear for a size scale of ~ 0.5 pc. Obviously, our value corresponds to a limitation of the star counts method with optical data and not to a real characteristic size scale of the cloud.

It is therefore natural to extrapolate, down to a minimum mass, the linear part of the relation $\log[M(A_V)]$ versus A_V to determine a maximum of extinction. This maximum is obtained using the regression line (3) and represents the higher extinction that can be measured, would the cloud be fractal at all size scales. As Blitz and Williams (1997) have shown, there is a characteristic size scale above which the density profile becomes steeper. The extrapolation of the linear relation gives, therefore, a lower limit for the densest core extinction. Derived values of A_V are presented in the 4th column of Table 1 and correspond to a minimum mass of $1M_{\odot}$. This minimum mass is a typical stellar mass and, an extrapolation toward lower masses would be meaningless.

Except for the Carina cloud, maxima are found in the range from 5.7 to 25.5 magnitudes of visual extinction with a median value of 10.6 magnitudes.

We stress the point that extinction can be larger. The ρ Ophiuchus cloud, for example, is known to show extinction peaks of about ~ 100 magnitudes (Casanova et al. 1995), whereas we obtain only 25.5 magnitudes. Nevertheless, this value compared to the 9.4 magnitudes effectively measured indicates that we need deeper optical observations or near-infrared data — such as those provided by the DENIS survey — to investigate more deeply the cloud. The Coalsack and Scorpius are the only clouds for which measured and extrapolated extinctions are similar (see Sect. 4).

3.3. Mass

Assuming a gas to dust ratio, the mass of a cloud can be obtained using the relation (Dickman 1978) :

$$M = (\alpha d)^2 \mu \frac{N_H}{A_V} \sum_i A_V(i)$$

where α is the angular size of a pixel map, d the distance to the cloud, μ the mean molecular weight corrected for helium abundance, and i is a pixel of the extinction map. Uncertainties on the determination of masses

come essentially from the distance which is always difficult to evaluate. Assuming a correct distance estimation, error resulting from magnitude uncertainties can be evaluated: an underestimation of 0.5 magnitude of visual extinction implies a reduction of the total mass of a factor ~ 2 . According to Savage and Mathis (1979), the gas to dust ratio is $\frac{N_H}{A_V} = 1.87 \times 10^{21} \text{ cm}^{-2} \cdot \text{mag}^{-1}$ where $N_H = N_{HI} + 2N_{H_2}$. Kim and Martin (1996) show that this value depends on the total to selective extinction ratio $R_V = A_V/E_{B-V}$. For $R_V = 5.3$, the gas to dust ratio would be divided by a factor 1.2. The value of R_V is supposed to be larger in molecular clouds than in the general interstellar medium but the variation with the extinction is not clearly established. So, I used the general value of 3.1 and the gas to dust ratio of Savage and Mathis. Mass of the cores of the clouds may, therefore, be overestimated by a factor ~ 1.2 .

In Fig. 10, the relation $\log[M(A_v)]$ vs. A_V extrapolated toward the zero extinction gives an estimation of the total mass of the cloud using Eq. (3). Masses obtained are shown in the Table 1. The median mass is $2900M_\odot$ and the range is from 80 to $5 \cdot 10^5 M_\odot$. Using expression (3), we also remark that half of the total mass is located outside the iso-extinction curve 1.0 magnitudes. This value is remarkably stable from cloud to cloud with a standard deviation of 0.3.

4. Remarks on individual clouds

4.1. Vela and Serpens

In the Vela and the Serpens clouds (Fig. 1 and 13, respectively), there is no linear relation between $\log[M(A_v)]$ and A_V . Extrapolation for the maximum of extinction or for the total mass estimations is not possible. However, mass lower limits can be obtained using the extinction map directly: $5.7 \cdot 10^4 M_\odot$ and $1.1 \cdot 10^5 M_\odot$ for Vela and Serpens, respectively. It is difficult to understand why there is no linear relation for these two clouds, even for low values of extinction.

4.2. Carina

The study of the Carina (Fig. 2) presents aberrant values for the slope of the line $\log[M(A_v)]$ (see Table 1). Consequently, the maximum of the extrapolated extinction, 82 magnitudes, cannot be trusted. The important reflection in the Carina region is probably responsible for the shape of the extinction map. Stars cannot be detected because of the reflection and thus, extinction cannot be derived from R star counts. Infrared data are requested to eliminate the contribution of the nebulae.

4.3. Musca–Chamaeleon

The Chamaeleon I has already been mapped with DENIS star counts in J band (Cambr sy et al. 1997) and the max-

imum of extinction was estimated to be ~ 10 magnitudes. Using B star counts we find here 5.2 magnitudes. This difference is normal since J is less sensitive to extinction than B . The important remark is that the extrapolated value for the extinction derived from B star counts is 12.9, consistent with the value obtained with J star counts. We obtain the same result for the Chamaeleon II cloud for which J star counts lead also to a maximum of about ~ 10 magnitudes whereas the extrapolated value from B counts is 12.3 magnitudes. Infrared data are definitely necessary to investigate the cores of the clouds.

Besides, the shape of the whole Musca–Chamaeleon extinction and the IRAS $100\mu\text{m}$ maps are very similar. Disregarding the far–infrared gradient produced by the heating by the galactic plane, there is a good match of the far–infrared emission and extinction contours and filamentary connections. This region is well adapted to study the correlation between the extinction and the far–infrared emission because there is no massive stars which heat the dust. The $100\mu\text{m}$ flux can, therefore, be converted in a relatively straightforward way into a column density unit using the $60/100\mu\text{m}$ colour temperature (Boulanger et al. 1998).

4.4. Coalsack and Scorpius

The extinction map of the Coalsack is displayed in Fig. 4. The edge of the cloud contains the brightest star of the Southern Cross ($\alpha = 12^h 26^m 36^s$, $\delta = -63^\circ 05' 57''$). This cloud is known to be a conglomerate of dust material, its distance is therefore difficult to estimate. Franco (1995) using Str mrgren photometry gives a distance of 150–200 pc. More recently Knude and Hog (1998) estimate a distance of 100–150 pc using Hipparcos data. Finally, I adopted an intermediate value of 150 pc to derive the mass of the Coalsack. Maximum extinction estimations for this cloud are 6.6 and 6.3 for the measured and the extrapolated values, respectively. The lowest limit for the maximum of extinction, as defined in Sect. 3.2, is reached, but no characteristic size scale has been found by studying the shape of $\log[M(A_v)]$ at high extinction. These values are too close, regarding their uncertainties, to reflect any evidence of a clumpy structure.

Nyman et al. (1989) have made a CO survey of the Coalsack cloud. They have divided the cloud into 4 regions. Regions I and II which correspond to the northern part of the area near α Crux, are well correlated with the extinction map. Nyman et al. have defined two other regions which have no obvious counterpart in extinction. Region III below -64° of declination in the western part of the cloud is not seen in the extinction map and this may result of a scanning defect of the plates. The same problem exists for the region IV which is a filament in the eastern part of the cloud at $\delta \simeq -64^\circ$.

The Scorpius cloud is located near the ρ Ophiuchus cloud (Fig. 9). The 120 pc distance used to derive its mass

Fig. 11. Extinction map of Orion, Monoceros I, Rosette, Monoceros II, Crossbones from R counts (J2000 coordinates)

Fig. 12. Extinction map of Taurus from R counts (J2000 coordinates)

Fig. 13. Extinction map of Serpens from R counts (J2000 coordinates)

is the ρ Ophiuchus distance (Knude and Hog 1998). As for the Coalsack cloud, measured and extrapolated extinction are similar : 6.4 and 7.0, respectively. But, no evidence of a characteristic size scale can be found. For both clouds, this result is not surprising since the maximum of measured extinction reaches the extrapolated value. Would dense cores with steeper extinction profile be found, the measured extinction would have been significantly greater than the extrapolated value.

4.5. *Corona Australis*

The extinction in this cloud has recently been derived using star counts on B plates by Andreatza and Vilas-Boas (1996). Our methods are very similar and we obtain, therefore, comparable results. The main difference comes from the most extinguished core. Since they use a regular grid, they cannot investigate cores where the mean distance between two stars is greater than their grid step. Consequently, they obtained a plateau where I find 4 distinct cores.

4.6. *IC5146*

CO observations are presented in Lada et al. (1994). The two eastern cores in the ^{13}CO map have only one counterpart in the extinction map because the bright nebula, Lynds 424, prevents the star detections in that region. Lada et al. (1994) also present an extinction map of a part of the cloud derived from $H - K$ colour excess observations. This colour is particularly well adapted for such investigations because, in one hand, infrared wavelengths allow deeper studies and, on the other hand, $H - K$ colour has a small dispersion versus the spectral type of stars. I obtain similar low iso-extinction contours but they reach a much greater maximum of visual extinction of about 20 magnitudes.

4.7. *Lupus*

New estimations of distance using Hipparcos data (Knude and Hog 1998) have led to locate the Lupus complex (Fig. 8) at only 100 pc from the Sun. Lupus turns out to be the most nearby star-forming cloud. This distance is used to estimate the complex mass but, it is important to remark that evidence of reddening suggests that dust material is present up to a distance of about 170 pc (Franco 1990). Masses could therefore be underestimated by a factor $\lesssim 3$

in these regions. The complex has been first separated into 4 clouds (Schwartz 1977), and then, a fifth cloud has been recently discovered using ^{13}CO survey (Tachihara et al. 1996). I have discovered, here, a sixth cloud which happens to be as massive as the Lupus I cloud, $\sim 10^4 M_\odot$ (assuming it is also located at 100 pc). The measured extinction for this cloud reaches 4.8 magnitudes.

The comparison between the ^{13}CO and the extinction map is striking, especially for the Lupus I cloud for which each core detected in the molecular observations has a counterpart in extinction. Mass estimations can be compared on condition that the same field is used for both maps. Moreover, ^{13}CO observations are less sensitive than B star counts for low extinction. The lower contour in the ^{13}CO map corresponds to a visual extinction of ~ 2 magnitudes. Using this iso-extinction contour to define the edge of the cloud and the same distance (150 pc) as Tachihara et al. (1996), I find a mass of $\sim 1300 M_\odot$ in agreement with their estimation of $1200 M_\odot$. Murphy et al. (1986) estimate the mass of the whole complex to be $\sim 3 \cdot 10^4 M_\odot$ using ^{12}CO observations and a distance of 130 pc. Using the same distance, I would obtain $4 \cdot 10^4 M_\odot$ ($2.3 \cdot 10^4 M_\odot$ for a 100 pc distance).

4.8. ρ *Ophiuchus*

Because of the important star formation activity of the inner part of the cloud, the IRAS flux at $100\mu\text{m}$ shows different structures of those seen in the extinction map. On the other hand, the 3 large filaments are present in both maps. Even if these regions are complex because several stars heat them, the comparison between the far-infrared emission and the extinction should allow to derive the dust temperature and a 3-dimensional representation of the cloud and of the stars involved in the heating. Unfortunately, uncertainties about the distances for these stars are too large (about 15%) and corresponds roughly to the cloud size.

4.9. *Orion*

Maddalena et al (1986) have published a large scale CO map of Orion and Monoceros R2. Masses derived from CO emission are consistent with those I obtain : $1.9 \cdot 10^5 M_\odot$ and $0.86 \cdot 10^5 M_\odot$ for Orion and Monoceros R2, respectively, from CO data and $3 \cdot 10^5 M_\odot$ and $1.2 \cdot 10^5 M_\odot$ from the extinction maps. The Orion B maps looks very alike. The Orion A maps show a significant difference near the

Trapezium ($\alpha = 5^h35^m$, $\delta = -5^\circ23'$) where the young stars pollute the star counts. The correlation between CO and extinction maps for Monoceros R2 is less striking, because of the star forming activity. It is clear that star clusters involve an underestimation of the extinction, but I would like to stress the point that the heating by a star cluster may also destroy the CO molecules. Estimation of the column density from star counts and from CO observations may, therefore, be substantially underestimated in regions such as the Trapezium.

4.10. Taurus

Onishi et al. (1996) have studied the cores in the Taurus cloud using a $C^{18}O$ survey. All of the 40 cores identified in their survey are also detected in the extinction map. Moreover, Abergel et al. (1994) have shown a strong correlation between the far-infrared and the ^{13}CO emission in that region. Despite the complexity of the Taurus structure (filaments, cores), it is a region, like the Chamaeleon complex, located at high galactic latitude ($b \simeq -16^\circ$), without complex stellar radiation field. This situation is highly favourable to a large scale comparison of CO, far-infrared and extinction maps.

5. Conclusion

Star counts technique is used since the beginning of the century and is still a very powerful way to investigate the distribution of solid matter in molecular clouds. Now, with the development of digital data, this technique become easy to use and can probe much larger areas. For all regions, we have assumed that all stars were background stars. The error resulting from this hypothesis can easily be estimated. Equation (1) can be written :

$$A_\lambda = \frac{1}{a} \log \left(\frac{S}{nb} \right) + cste(D_{ref})$$

where S is the surface which contains nb stars. If 50% of the stars are foreground stars, the difference between the real extinction and the extinction which assumes all background stars is :

$$\Delta A_\lambda = \frac{1}{a} \log 2$$

That corresponds to ~ 0.6 or ~ 1.1 magnitudes of visual extinction whether star counts are done using B or R band, respectively. Fortunately, most of the clouds are located at small or intermediate distances to the Sun (except the Carina at 2500 pc) and this effect is probably small, at least for low extinction. The good agreement between mass derived from extinction or from CO data argues in that favour.

Stars physically associated to the clouds are more problematic because they are located precisely close to the extinction cores. Young objects are generally faint in the

optical band so this problem may be neglected for optical counts. This is no longer true with near-infrared data for which young objects must be removed before the star counts. We obtain extinction map with a spatial resolution always adapted to the local densities which are typically about $\sim 1'$ for the outer part of cloud and $\sim 10'$ for the most extinguished regions where the stellar density becomes very low, i.e. $\lesssim 1000$ stars.deg $^{-2}$. These maps allow the estimation of the total mass of the cloud by extrapolation of the distribution of matter with the extinction. It appears that mass concentrated in the regions of low extinction represents an important part of the total mass of a cloud (1/2 is contained in regions of extinction lower than 1 magnitude).

Extrapolation of the distribution of matter in highly extinguished areas is more risky. Star counts method give a relation for which masses are underestimated in the cores of the cloud for a well understood reason: estimation of the local density requires to pick up enough stars and thus, to use larger area because of the low number density. Moreover a characteristic size scale in the distribution of matter (Blitz and Williams 1997) indicates the presence of the lower limit of the fractal cloud structure. For this size scale the linear extrapolation used in Fig. 10 also underestimates the real mass and extinction. Despite this difficulty, the extrapolated extinction is useful to estimate the *saturation* level in the extinction map, but it is important to keep in mind that extinction can be much larger in small cores.

Finally, the examination of the relation between mass and extinction is useful to check what we are measuring. The Carina cloud show an aberrant slope (Table 1) which is a strong indication that the map cannot be directly interpreted as an *extinction* map. In that case, the elimination of reflection nebulae is probably a solution and therefore, near-infrared data are requested to investigate the extinction. For the Vela and the Serpens cloud, the absence of linear part is not understood and reflection is not the solution in these regions.

Acknowledgements. I warmly thank N. Epchtein for initiating this study and for his critical reading of the manuscript which helped to clarify this paper. The *Centre de Donn ees astronomiques de Strasbourg* (CDS) is also thanked for accessing to the USNO data.

References

- Abergel A., Boulanger F., Mizuno A., et al., 1994, ApJ 423, L59
- Andreazza C.M., Vilas-Boas J.W.S., 1996, A&AS 116, 21
- Bazell D., D esert F.X., 1988, ApJ 333, 353
- Bernard J.P., Boulanger F., Puget J.L., 1993, A&A 277, 609
- Blitz L., Williams J.P., 1997, ApJ 488, L145
- Bok B.J., 1956, AJ 61, 309

- Boulanger F., Bronfman L., Dame T., et al., 1998, *A&A* 332, 273
- Cambrésy L., 1998, *The Impact of Near Infrared Sky Surveys on Galactic and Extragalactic Astronomy*, ed. N. Epchtein, vol. 230 of ASSL series, 157–163, Kluwer Academic Publishers
- Cambrésy L., Epchtein N., Copet E., et al., 1997, *A&A* 324, L5
- Cardelli J., Geoffrey C., Mathis J., 1989, *ApJ* 345, 245
- Casanova S., Montmerle T., Feigelson E.D., et al., 1995, *ApJ* 439, 752
- Dickman R.L., 1978, *AJ* 83, 363
- Duncan A.R., Stewart R.T., Haynes R.F., et al., 1996, *MNRAS* 280, 252
- Elmegreen B.G., Falgarone E., 1996, *ApJ* 471, 816
- Feinstein A., 1995, *Revista Mexicana de Astronomia y Astrofisica Conference Series* 2, 57
- Franco G.A.P., 1990, *A&A* 227, 499
- Franco G.A.P., 1995, *A&AS* 114, 105
- Gregorio Hetem J., Sanzovo G., Lépine J., 1988, *A&AS* 76, 347
- Hetem A. J., Lépine J.R.D., 1993, *A&A* 270, 451
- Hoffleit D., Jaschek C., 1991, New Haven, Conn.: Yale University Observatory, 5th rev.ed., edited by Hoffleit, D.; Jaschek, C. (coll.)
- Kenyon S.J., Dobrzycka D., Hartmann L., 1994, *AJ* 108, 1872
- Kim S.H., Martin P., 1996, *ApJ* 462, 296
- Knude J., Hog E., 1998, *A&A* 338, 897
- Lada C., Lada E., Clemens D., et al., 1994, *ApJ* 429, 694
- Larson R.B., 1995, *MNRAS* 272, 213
- Maddalena R.J., Morris M., Moscowitz J., et al., 1986, *ApJ* 303, 375
- Mizuno A., Hayakawa T., Yamaguchi N., et al., 1998, *ApJ* 507, L83
- Monet D., 1996, *BAAS* 188, 5404
- Murphy D.C., Cohen R., May J., 1986, *A&A* 167, 234
- Nyman L.A., Bronfman L., Thaddeus P., 1989, *A&A* 216, 185
- Onishi T., Mizuno A., Kawamura A., et al., 1996, *ApJ* 465, 815
- Savage B.D., Mathis J.S., 1979, *ARA&A* 17, 73
- Schwartz R.D., 1977, *ApJS* 35, 161
- Straižys V., Černis K., Bartašiūtė S., 1996, *Baltic Astronomy* 5, 125
- Tachihara K., Dobashi K., Mizuno A., et al., 1996, *PASJ* 48, 489
- Turner D.G., 1976, *ApJ* 210, 65
- Whittet D., Prusti T., Franco G., et al., 1997, *A&A* 327, 1194
- Wolf M., 1923, *Astron. Nachr.* 219, 109

This figure "fig1.gif" is available in "gif" format from:

<http://arxiv.org/ps/astro-ph/9903149v1>

This figure "fig2.gif" is available in "gif" format from:

<http://arxiv.org/ps/astro-ph/9903149v1>

This figure "fig3.gif" is available in "gif" format from:

<http://arxiv.org/ps/astro-ph/9903149v1>

This figure "fig4.gif" is available in "gif" format from:

<http://arxiv.org/ps/astro-ph/9903149v1>

This figure "fig5.gif" is available in "gif" format from:

<http://arxiv.org/ps/astro-ph/9903149v1>

This figure "fig6.gif" is available in "gif" format from:

<http://arxiv.org/ps/astro-ph/9903149v1>

This figure "fig7.gif" is available in "gif" format from:

<http://arxiv.org/ps/astro-ph/9903149v1>

This figure "fig8.gif" is available in "gif" format from:

<http://arxiv.org/ps/astro-ph/9903149v1>

This figure "fig9.gif" is available in "gif" format from:

<http://arxiv.org/ps/astro-ph/9903149v1>

This figure "fig11.gif" is available in "gif" format from:

<http://arxiv.org/ps/astro-ph/9903149v1>

This figure "fig12.gif" is available in "gif" format from:

<http://arxiv.org/ps/astro-ph/9903149v1>

This figure "fig13.gif" is available in "gif" format from:

<http://arxiv.org/ps/astro-ph/9903149v1>